Vietnam Journal of Mechanics, VAST, Vol. 31, No. 4 &0 (2009), pp. 279 – 292

# A NEW PRISMATIC SOLID-SHELL ELEMENT 'SHB6': ASSUMED-STRAIN FORMULATION AND EVALUATION ON BENCHMARK PROBLEMS

**Vuong-Dieu Trinh**[1], **Farid Abed-Meraim**[1], **Alain Combescure**[2]
[1] *LPMM UMR CNRS 7554, Arts et Métiers ParisTech,*
*4 rue Augustin Fresnel, 57078 Metz*
[2] *LaMCoS UMR CNRS 5259, INSA-Lyon,*
*18, 20 rue des Sciences, 69621 Villeurbanne, France*

**Abstract.** In this paper, the formulation of a new six-node solid–shell element denoted (SHB6) is proposed. This prismatic element is based on a purely three-dimensional approach, and hence has displacements as the only degrees of freedom. A reduced integration scheme is adopted consisting of one-point in-plane quadrature and an arbitrary number of integration points, with a minimum number of two, distributed along the 'thickness' direction. Moreover, in order to enhance its performance and to greatly reduce most locking effects, specific projections are introduced based on the assumed-strain method. The resulting derivation can then be used to model thin structural problems, while taking into account the various through-thickness phenomena. A careful analysis of potential stiffness matrix rank deficiencies reveals that no hourglass modes need to be controlled. However, without assumed-strain method, the element exhibits some shear and thickness-type locking, which is common in linear triangular elements associated with constant strain states. After the formulation of the element is detailed, its performance is assessed through a set of representative benchmark problems illustrating its capabilities in various situations. More specifically, this prismatic solid–shell element proves to be an essential complement to the SHB8PS hexahedral element in meshing arbitrarily complex geometries.

**Keywords**. solid–shell element shb6, shear and thickness locking, assumed-strain method, hourglass modes, benchmark problems.

## 1. INTRODUCTION

Accuracy and efficiency of finite elements (FE) are the main features expected with the ever-growing resort to FE-based software packages. For the three-dimensional analysis of structural problems, the development of effective eight-node solid–shell finite elements has been a major objective over the last decade as revealed by several recently published contributions [1–5]. However, to be able to mesh complex geometries and with the advent of free mesh generation tools not generating only hexahedrons, the development of prismatic solid–shell elements is made necessary. Note that most of the methods developed earlier

[1] *vuong-dieu.trinh@metz.ensam.fr*, *farid.abed-meraim@metz.ensam.fr*
[2] *hdb@lms.polytechnique.fr, stephanie.chaillat@cc.gatech.edu*, *alain.combescure@insa-lyon.fr*

were based on the enhanced assumed strain method proposed by Simo and co-workers [6–8], and consisted of either the use of a conventional integration scheme with appropriate control of all locking phenomena or the application of a reduced integration technique with associated hourglass control. Both approaches have been extensively investigated and evaluated in various structural applications, as reported in numerous references [9–15]. This paper presents the formulation of a six-node solid–shell finite element called SHB6. It consists of a thick shell obtained from a purely three-dimensional approach. The assumed-strain method is adopted together with an in-plane reduced integration scheme using a minimum number of two integration points along the thickness direction. The three-dimensional elastic constitutive law is also modified so that a shell-like behavior is intended for the element and in order to alleviate shear and thickness-type locking.

Because reduced integration schemes are known to introduce spurious mechanisms associated with zero energy, an adequate hourglass control is generally needed. An effective treatment for kinematic modes was proposed by Belytschko and Bindeman [1], with a physical stabilization procedure to correct the rank deficiency of eight-node hexahedral elements. As the SHB6 is also under-integrated, a detailed eigenvalue analysis of the element stiffness matrix is carried out. We demonstrate that the kernel of this stiffness matrix only reduces to rigid body movements and hence, in contrast to the eight-node solid–shell element (SHB8PS), the SHB6 element does not require stabilization. Nevertheless, we propose modifications, based on the well-known assumed-strain method [1], for the discrete gradient operator of the element in order to improve its convergence rate.

Indeed, as revealed by numerical evaluations of the SHB6 element, its original displacement-based version, without modification of its discrete gradient operator, suffered from shear and thickness locking. To attenuate these locking phenomena, several modifications have been introduced into the formulation of the SHB6 element following the assumed-strain method adopted by Belytschko and Bindeman [1]. Finally, a variety of popular benchmark problems has been performed and good results have been obtained when compared to other triangular-based elements available in the literature. In particular, it is shown that this new element plays a useful role as a complement to the SHB8PS hexahedral element, which enables one to mesh arbitrary geometries. Examples using both SHB6 and SHB8PS elements demonstrate the advantage of mixing these two solid–shell elements.

## 2. FORMULATION OF THE SHB6 FINITE ELEMENT

The SHB6 element is a prismatic continuum shell, based on a purely three-dimensional approach, with six nodes and only three displacement degrees of freedom per node. It is provided with a special direction called the ‘thickness’, normal to the mean plane of the triangle. A reduced integration scheme is adopted with at least two integration points along the thickness direction and only one point in the in-plane directions. Figure 1 shows the SHB6 reference geometry as well as the location of its integration points.

### 2.1. Kinematics and interpolation

The SHB6 is a linear, isoparametric element. Its spatial coordinates $x_i$ and displacements $u_i$ are respectively related to the nodal coordinates $x_{iI}$ and displacements $u_{iI}$

through the linear shape functions $(N_1, N_2, ..., N_6)$ as follows:

$$\begin{aligned} x_i &= x_{iI} N_I(\xi,\eta,\zeta) = \sum_{I=1}^{6} x_{iI} N_I(\xi,\eta,\zeta), \\ u_i &= u_{iI} N_I(\xi,\eta,\zeta) = \sum_{I=1}^{6} u_{iI} N_I(\xi,\eta,\zeta) \end{aligned} \tag{1}$$

Hereafter, unless specified otherwise, the implied summation convention for repeated indices will be adopted. Lowercase indices $i$ vary from one to three and represent spatial coordinate directions. Uppercase indices $I$ vary from one to six and correspond to element nodes. The tri-linear isoparametric shape functions $N_I$ are:

$$\begin{aligned} N(\xi,\eta,\zeta) = \frac{1}{2}[&(1-\zeta)(1-\xi-\eta) \quad (1-\zeta)\xi \quad (1-\zeta)\eta \\ &(1+\zeta)(1-\xi-\eta) \quad (1+\zeta)\xi \quad (1+\zeta)\eta] \\ \xi = [0,1]; \quad &\eta = [0,1-\xi]; \quad \zeta = [-1,1] \end{aligned} \tag{2}$$

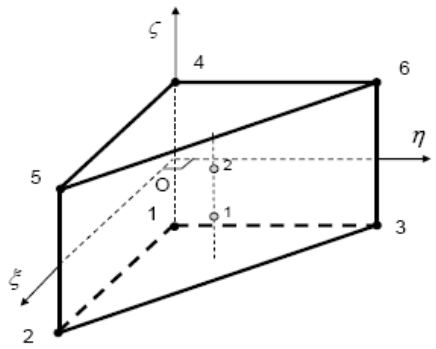


*Fig. 1.* Reference geometry of the SHB6 element and example of quadrature using two integration points

## 2.2. Discrete gradient operator

Using some mathematical derivations, similarly to the procedure for the SHB8PS development reported in [16], we can explicitly express the relationship between the linear part of the strain field and the nodal displacements. Combining Eqs. (1) and (2) leads to the following expansion for the displacement field:

$$\begin{cases} u_i(\xi,\eta,\zeta,x,y,z) = a_{0i} + a_{1i}x + a_{2i}y + a_{3i}z + c_{1i}h_1 + c_{2i}h_2 \\ i = 1,2,3 \\ h_1 = \zeta\eta, \ h_2 = \zeta\xi \end{cases} \tag{3}$$

Evaluating this last equation at the element nodes yields the following three six-equation systems:

$$\mathbf{d}_i = a_{0i}\mathbf{s} + a_{1i}\mathbf{x}_1 + a_{2i}\mathbf{x}_2 + a_{3i}\mathbf{x}_3 + c_{1i}\mathbf{h}_1 + c_{2i}\mathbf{h}_2 \ ; \ i = 1,2,3 \tag{4}$$

where the six-component vectors $\mathbf{d}_i$ and $\mathbf{x}_i$ respectively denote the nodal displacements and coordinates, and vectors $\mathbf{s}$ and $\mathbf{h}_\alpha \quad (\alpha = 1, 2)$ are given by:

$$\begin{cases} \mathbf{s}^T = (\ 1,\ 1,\ 1,\ 1,\ 1,\ 1) \\ \mathbf{h}_1^T = (0, 0, -1, 0, 0, 1) \\ \mathbf{h}_2^T = (0, -1, 0, 0, 1, 0) \end{cases} \tag{5}$$

Let consider now the derivatives of the shape functions evaluated at the origin of the reference frame:

$$\mathbf{b}_i = \mathbf{N}_{,i}(0) = \frac{\partial \mathbf{N}}{\partial x_i}_{|\xi\,=\,\eta\,=\,\zeta\,=\,0} \quad i = 1, 2, 3\ \textit{Hallquist Form} \tag{6}$$

Explicit expressions of vectors $\mathbf{b}_i$ can be derived by algebra together with useful orthogonality relations:

$$\begin{cases} \mathbf{b}_i^T \cdot \mathbf{h}_\alpha = 0\ ,\ \mathbf{b}_i^T \cdot \mathbf{s} = 0\ ,\ \mathbf{b}_i^T \cdot \mathbf{x}_j = \delta_{ij} \\ \mathbf{h}_\alpha^T \cdot \mathbf{s} = 0\ ,\ \mathbf{h}_\alpha^T \cdot \mathbf{h}_\beta = 2\delta_{\alpha\beta} \\ i, j = 1, ..., 3\ \alpha,\beta = 1,2 \end{cases} \tag{7}$$

These orthogonality conditions allow the constants $a_{ki}$ and $c_{\alpha i}$ to be determined by scalar products:

$$\begin{cases} a_{ki} = \mathbf{b}_k^T \cdot \mathbf{d}_i\ ,\ c_{\alpha i} = \gamma_\alpha^T \cdot \mathbf{d}_i \\ \text{where: } \gamma_\alpha = \frac{1}{2}\left[\mathbf{h}_\alpha - \sum_{j=1}^{3} (\mathbf{h}_\alpha^T \cdot \mathbf{x}_j)\mathbf{b}_j\right] \end{cases} \tag{8}$$

which, combined with Eq. (3), lead to the following convenient form for the displacement field:

$$u_i = a_{0i} + (x_1\mathbf{b}_1^T + x_2\mathbf{b}_2^T + x_3\mathbf{b}_3^T + h_1\gamma_1^T + h_2\gamma_2^T) \cdot \mathbf{d}_i \tag{9}$$

The symmetric part of the displacement gradient is then obtained by differentiating this last equation:

$$\nabla_s(\mathbf{u}) = \mathbf{B} \cdot \mathbf{d}$$

$$\nabla_s(\mathbf{u}) = \begin{bmatrix} u_{x,x} \\ u_{y,y} \\ u_{z,z} \\ u_{x,y} + u_{y,x} \\ u_{y,z} + u_{z,y} \\ u_{x,z} + u_{z,x} \end{bmatrix},\ \mathbf{d} = \begin{bmatrix} \mathbf{d}_x \\ \mathbf{d}_y \\ \mathbf{d}_z \end{bmatrix},$$

$$\mathbf{B} = \begin{bmatrix} \mathbf{b}_x^T + h_{\alpha,x}\gamma_\alpha^T & \mathbf{0} & \mathbf{0} \\ \mathbf{0} & \mathbf{b}_y^T + h_{\alpha,y}\gamma_\alpha^T & \mathbf{0} \\ \mathbf{0} & \mathbf{0} & \mathbf{b}_z^T + h_{\alpha,z}\gamma_\alpha^T \\ \mathbf{b}_y^T + h_{\alpha,y}\gamma_\alpha^T & \mathbf{b}_x^T + h_{\alpha,x}\gamma_\alpha^T & \mathbf{0} \\ \mathbf{0} & \mathbf{b}_z^T + h_{\alpha,z}\gamma_\alpha^T & \mathbf{b}_y^T + h_{\alpha,y}\gamma_\alpha^T \\ \mathbf{b}_z^T + h_{\alpha,z}\gamma_\alpha^T & \mathbf{0} & \mathbf{b}_x^T + h_{\alpha,x}\gamma_\alpha^T \end{bmatrix} \tag{10}$$

This form of the discrete gradient operator $\mathbf{B}$ is very useful because it allows each of the non-constant strain modes to be handled separately to build an appropriate assumed-strain field. In addition, it can be shown that the $\gamma_\alpha$ vectors involved in this operator

satisfy the following orthogonality relations:

$$\gamma_\alpha^T \cdot \mathbf{x}_j = 0,\ \gamma_\alpha^T \cdot \mathbf{h}_\beta = \delta_{\alpha\beta} \tag{11}$$

These conditions will prove to be helpful in the subsequent analysis of stiffness matrix rank deficiencies.

### 2.3. Variational principle

The expression of the weak form of the Hu–Washizu mixed variational principle, as extended to non-linear solid mechanics by Fish and Belytschko [17], reads for a single finite element:

$$\delta\pi(\mathbf{v}, \dot{\bar{\varepsilon}}, \bar{\sigma}) = \int_{\Omega_e} \delta\dot{\bar{\varepsilon}}^T \cdot \sigma \ d\Omega + \delta \int_{\Omega_e} \bar{\sigma}^T \cdot \left(\nabla_s(\mathbf{v}) - \dot{\bar{\varepsilon}}\right) d\Omega - \delta\dot{\mathbf{d}}^T \cdot \mathbf{f}^{ext} = 0 \tag{12}$$

where $\delta$ denotes a variation, $\mathbf{v}$ the velocity gradient, $\dot{\bar{\varepsilon}}$ the assumed-strain rate, $\bar{\sigma}$ the interpolated stress, $\sigma$ the stress evaluated by the constitutive equations, $\dot{\mathbf{d}}$ the nodal velocities, $\mathbf{f}^{ext}$ the external nodal forces, and $\nabla_s(\mathbf{v})$ the symmetric part of the velocity gradient. In the simplified form of this principle, as described by Simo and Hughes [18], the assumed stress field is chosen to be orthogonal to the difference between the symmetric part of the displacement gradient and the assumed strain field, leading to:

$$\delta\pi(\dot{\bar{\varepsilon}}) = \int_{\Omega_e} \delta\dot{\bar{\varepsilon}}^T \cdot \sigma \ d\Omega - \delta\dot{\mathbf{d}}^T \cdot \mathbf{f}^{ext} = 0 \tag{13}$$

Therefore, the discrete equations only require the interpolation of the velocity and the assumed-strain filed. The latter is expressed in terms of a $\bar{\mathbf{B}}$ matrix, projected starting from the standard $\mathbf{B}$ operator:

$$\dot{\bar{\varepsilon}}(x,t) = \bar{\mathbf{B}}(x) \cdot \dot{\mathbf{d}}(t) \tag{14}$$

Replacing (14) in the variational principle (13), leads to the following expression for the internal forces:

$$\mathbf{f}^{int} = \int_{\Omega_e} \bar{\mathbf{B}}^T \cdot \sigma(\dot{\bar{\varepsilon}}) \ d\Omega \tag{15}$$

For linear elastic problems, the element stiffness matrix takes the following form:

$$\mathbf{K}_e = \int_{\Omega_e} \bar{\mathbf{B}}^T \cdot \mathbf{C} \cdot \bar{\mathbf{B}} \ d\Omega \tag{16}$$

Note that similarly to the SHB8PS element [16], an improved plane-stress type constitutive law is adopted here, in order to enhance the element immunity with regard to thickness locking.

### 2.4. Hourglass mode analysis

Hourglass mechanisms are spurious zero-energy modes that are generated by the reduced integration. Therefore, the analysis of hourglass modes is equivalent to the investigation of stiffness matrix rank deficiency. Within a displacement-based approach, a zero-energy mode is a vector $\mathbf{h}_g$ that satisfies:

$$\mathbf{B}(\zeta_I) \cdot \mathbf{h}_g = \mathbf{0} \; ; \; I = 1, ..., n_{int} \tag{17}$$

We can easily demonstrate that the following $(e_i, \; i = 1, ..., 18)$ vectors are linearly independent, and hence, they form a basis for the vector space of the discretized displacements:

$$\begin{aligned}
&e_1 = \begin{pmatrix} \mathbf{s} \\ \mathbf{0} \\ \mathbf{0} \end{pmatrix}, \quad e_2 = \begin{pmatrix} \mathbf{0} \\ \mathbf{s} \\ \mathbf{0} \end{pmatrix}, \; e_3 = \begin{pmatrix} \mathbf{0} \\ \mathbf{0} \\ \mathbf{s} \end{pmatrix}, \quad e_4 = \begin{pmatrix} \mathbf{x} \\ \mathbf{0} \\ \mathbf{0} \end{pmatrix}, \quad e_5 = \begin{pmatrix} \mathbf{0} \\ \mathbf{x} \\ \mathbf{0} \end{pmatrix}, \quad e_6 = \begin{pmatrix} \mathbf{0} \\ \mathbf{0} \\ \mathbf{x} \end{pmatrix}, \\
&e_7 = \begin{pmatrix} \mathbf{x} \\ \mathbf{0} \\ \mathbf{0} \end{pmatrix}, \quad e_8 = \begin{pmatrix} \mathbf{0} \\ \mathbf{x} \\ \mathbf{0} \end{pmatrix}, \quad e_9 = \begin{pmatrix} \mathbf{0} \\ \mathbf{0} \\ \mathbf{x} \end{pmatrix}, \quad e_{10} = \begin{pmatrix} \mathbf{x} \\ \mathbf{0} \\ \mathbf{0} \end{pmatrix}, \; e_{11} = \begin{pmatrix} \mathbf{0} \\ \mathbf{x} \\ \mathbf{0} \end{pmatrix}, \; e_{12} = \begin{pmatrix} \mathbf{0} \\ \mathbf{0} \\ \mathbf{x} \end{pmatrix}, \\
&e_{13} = \begin{pmatrix} \mathbf{h}_1 \\ \mathbf{0} \\ \mathbf{0} \end{pmatrix}, e_{14} = \begin{pmatrix} \mathbf{0} \\ \mathbf{h}_1 \\ \mathbf{0} \end{pmatrix}, e_{15} = \begin{pmatrix} \mathbf{0} \\ \mathbf{0} \\ \mathbf{h}_1 \end{pmatrix}, e_{16} = \begin{pmatrix} \mathbf{h}_2 \\ \mathbf{0} \\ \mathbf{0} \end{pmatrix}, e_{17} = \begin{pmatrix} \mathbf{0} \\ \mathbf{h}_2 \\ \mathbf{0} \end{pmatrix}, e_{18} = \begin{pmatrix} \mathbf{0} \\ \mathbf{0} \\ \mathbf{h}_2 \end{pmatrix}
\end{aligned} \tag{18}$$

Assuming that vector $\mathbf{h}^g$ belongs to the stiffness kernel, one can expand it in terms of the base vectors:

$$\mathbf{h}^g = \sum_{i=1}^{18} c_i e_i \tag{19}$$

Combining Eqs. (19), (17), and (10), and taking advantage of orthogonality conditions (7), one obtains:

$$\begin{pmatrix}
c_4 + h_{1,x}(\xi_I)\, c_{13} + h_{2,x}(\xi_I)\, c_{16} \\
c_8 + h_{1,y}(\xi_I)\, c_{14} + h_{2,y}(\xi_I)\, c_{17} \\
c_{12} + h_{1,z}(\xi_I)\, c_{15} + h_{2,z}(\xi_I)\, c_{18} \\
c_5 + c_7 + h_{1,y}(\xi_I)\, c_{13} + h_{1,x}(\xi_I)\, c_{14} + h_{2,y}(\xi_I)\, c_{16} + h_{2,x}(\xi_I)\, c_{17} \\
c_9 + c_{11} + h_{1,z}(\xi_I)\, c_{14} + h_{1,y}(\xi_I)\, c_{15} + h_{2,z}(\xi_I)\, c_{17} + h_{2,y}(\xi_I)\, c_{18} \\
c_6 + c_{10} + h_{1,z}(\xi_I)\, c_{13} + h_{1,x}(\xi_I)\, c_{15} + h_{2,z}(\xi_I)\, c_{16} + h_{2,x}(\xi_I)\, c_{18}
\end{pmatrix} = 0; \tag{20}$$

$I = 1, \ldots, n_{\text{int}}$

Evaluating the above equation at the $n_{int}$ different integration points of the SHB6 implies that:

$$\begin{cases} c_4 = c_{13} = c_{16} = 0 \\ c_8 = c_{14} = c_{17} = 0 \\ c_{12} = c_{15} = c_{18} = 0 \\ c_5 + c_7 = 0 \\ c_9 + c_{11} = 0 \\ c_6 + c_{10} = 0 \end{cases} \tag{21}$$

and hence:

$$\mathbf{h}^g = c_1 \begin{pmatrix} \mathbf{s} \\ \mathbf{0} \\ \mathbf{0} \end{pmatrix} + c_2 \begin{pmatrix} \mathbf{0} \\ \mathbf{s} \\ \mathbf{0} \end{pmatrix} + c_3 \begin{pmatrix} \mathbf{0} \\ \mathbf{0} \\ \mathbf{s} \end{pmatrix} + c_5 \begin{pmatrix} \\ \mathbf{0} \\ \\ \end{pmatrix} () \tag{22}$$

This last equation reveals that the kernel of the stiffness matrix only consists of the usual six rigid body modes (three translations and three rotations), and thus no rank deficiency is observed. It should be noted that this formulation of the SHB6 element is valid for any set of $n_{\text{int}}$ integration points located along the same line $\xi_I = \eta_I = \frac{1}{3},\ \zeta_I, \quad I = 1, ..., n_{\text{int}}$, and comprising at least two integration points ($n_{int} \geq 2$).

### 2.5. Assumed-strain formulation for the SHB6

In this section, the discrete gradient operator $\mathbf{B}$ will be projected onto an appropriate subspace in order to eliminate different locking phenomena; the projected operator will be denoted $\bar{\mathbf{B}}$. It has been shown that this assumed-strain method is consistent, from a variational perspective, with the Hu–Washizu principle as long as the stress interpolation is appropriately chosen (see Simo and Hughes [18]). However, this variational justification of the assumed-strain method does not provide a general and systematic way to derive adequate assumed-strain fields, and a specific analysis of locking must be conducted for each new element developed based on this approach. For this purpose, we propose a projection scheme that is both effective and simple (see [1] for further details). This consists first of decomposing the discrete gradient operator $\mathbf{B}$ into two parts as follows:

$$\mathbf{B} = \mathbf{B}_1 + \mathbf{B}_2. \tag{23}$$

In this additive decomposition, the first part, $\mathbf{B}_1$, contains the gradients in the element mid-plane (membrane terms of the deformation) as well as the normal strains, whereas the second part, $\mathbf{B}_2$, incorporates the gradients associated with the transverse shear strains:

$$\mathbf{B}_1 = \begin{bmatrix} \mathbf{b}_x^T + h_{\alpha,x}\gamma_\alpha^T & \mathbf{0} & \mathbf{0} \\ \mathbf{0} & \mathbf{b}_y^T + h_{\alpha,y}\gamma_\alpha^T & \mathbf{0} \\ \mathbf{0} & \mathbf{0} & \mathbf{b}_z^T + h_{\alpha,z}\gamma_\alpha^T \\ \mathbf{b}_y^T + h_{\alpha,y}\gamma_\alpha^T & \mathbf{b}_x^T + h_{\alpha,x}\gamma_\alpha^T & \mathbf{0} \\ \mathbf{0} & \mathbf{0} & \mathbf{0} \\ \mathbf{0} & \mathbf{0} & \mathbf{0} \end{bmatrix} \tag{24}$$

$$\mathbf{B}_2 = \begin{bmatrix} \mathbf{0} & \mathbf{0} & \mathbf{0} \\ \mathbf{0} & \mathbf{0} & \mathbf{0} \\ \mathbf{0} & \mathbf{0} & \mathbf{0} \\ \mathbf{0} & \mathbf{0} & \mathbf{0} \\ \mathbf{0} & \mathbf{b}_z^T + h_{\alpha,z}\gamma_\alpha^T & \mathbf{b}_y^T + h_{\alpha,y}\gamma_\alpha^T \\ \mathbf{b}_z^T + h_{\alpha,z}\gamma_\alpha^T & \mathbf{0} & \mathbf{b}_x^T + h_{\alpha,x}\gamma_\alpha^T \end{bmatrix} \tag{25}$$

It has been observed, from numerical experiments, that the main locking effects in the SHB6 element originate from the transverse shears. Therefore, we choose an integration scheme that enables us to reduce the associated fraction in the total strain energy. In order to do this, matrix $\mathbf{B}_2$ is projected as follows:

$$\bar{\mathbf{B}}_2 = \varepsilon \mathbf{B}_2 \tag{26}$$

where $\varepsilon$ is a shear scaling factor. By introducing the additive decomposition (23) of the $\mathbf{B}$ operator into Eq. (16) and making use of projection (26), the stiffness matrix becomes:

$$\mathbf{K}_e = \int_{\Omega_e} \mathbf{B}_1^T \cdot \mathbf{C} \cdot \mathbf{B}_1 \, d\Omega + \int_{\Omega_e} \mathbf{B}_1^T \cdot \mathbf{C} \cdot \bar{\mathbf{B}}_2 \, d\Omega + \int_{\Omega_e} \bar{\mathbf{B}}_2^T \cdot \mathbf{C} \cdot \mathbf{B}_1 \, d\Omega + \int_{\Omega_e} \bar{\mathbf{B}}_2^T \cdot \mathbf{C} \cdot \bar{\mathbf{B}}_2 \, d\Omega \tag{27}$$

which can be simply written as: $\mathbf{K}_e = \mathbf{K}_1 + \mathbf{K}_2$. The first term, $\mathbf{K}_1$, which is not affected by projection, is evaluated at the integration points as defined above:

$$\mathbf{K}_1 = \int_{\Omega_e} \mathbf{B}_1^T \cdot \mathbf{C} \cdot \mathbf{B}_1 \, d\Omega = \sum_{I=1}^{n_{int}} \omega(\zeta_I) J(\zeta_I) \mathbf{B}_1^T(\zeta_I) \cdot \mathbf{C} \cdot \mathbf{B}_1(\zeta_I) \tag{28}$$

The second term, $\mathbf{K}_2$, embodies all the projection and reads:

$$\mathbf{K}_2 = \int_{\Omega_e} \mathbf{B}_1^T \cdot \mathbf{C} \cdot \bar{\mathbf{B}}_2 \, d\Omega + \int_{\Omega_e} \bar{\mathbf{B}}_2^T \cdot \mathbf{C} \cdot \mathbf{B}_1 \, d\Omega + \int_{\Omega_e} \bar{\mathbf{B}}_2^T \cdot \mathbf{C} \cdot \bar{\mathbf{B}}_2 \, d\Omega \tag{29}$$

The particular choice of additive decomposition, Eqs. (24) and (25), together with projection (26), yields a simplified form for the second part of the stiffness matrix $\mathbf{K}_2$. Indeed, with these choices the first two terms, i.e. cross-terms, in the right-hand side of Eq. (29) vanish, and matrix $\mathbf{K}_2$ simply reduces to:

$$\mathbf{K}_2 = \int_{\Omega_e} \bar{\mathbf{B}}_2^T \cdot \mathbf{C} \cdot \bar{\mathbf{B}}_2 \, d\Omega \tag{30}$$

The identification of the shear scaling factor $\varepsilon$ in Eq. (26) has been carried out through numerical experiments, and the selected value for this parameter is found to be one half. This value is motivated by extensive testing on a variety of popular test problems, and it leads to reasonably good behavior for the element in most of the benchmark problems that have been tested.

## 3. NUMERICAL RESULTS AND ASSESSMENT

In this section, the evaluation of the SHB6 element will be carried out through several popular benchmark problems. For each test problem, the obtained results are compared with the reference solution from literature and with the solutions given by both the standard three-dimensional six-node prism element PRI6 and the unmodified SHB6 element (i.e., without assumed-strain projection). To avoid confusion, the assumed-strain projected version of the SHB6 will be denoted SHB6$^{bar}$. Note that this first selection of numerical examples is restricted to linear elastic problems and is mainly intended to assess the performance of the element in bending-dominated problems and to illustrate the benefit of mixing hexahedral and prismatic solid–shell elements such as the SHB6$^{bar}$ and SHB8PS. In all numerical tests, a single element with only two integration points is used through the thickness. In the tables reporting the convergence results, the meshes are indicated by the number of subdivisions in each direction (length, width), and the total element number is then doubled, since each rectangle is divided into two triangles.

### 3.1. Twisted cantilever beam

This test has been introduced by MacNeal and Harder [19] and has been extensively used to test finite element performance in cases of warped configurations. It is considered now as a reference shell test. The geometry is twisted by an angle of 90 ° between the two ends of the beam. This distorts the elements and thus increases the severity of the test. Figure 2 shows the geometry of the twisted beam, the boundary conditions and the applied loading. The left-side end of the beam is clamped and a unit in-plane shear load, $P = 1$, is applied at its right-side end in the $z$-direction. The geometric and material parameters for this problem are listed in Table 1. The reference tip displacement in the loading direction $Oz$ is given in [19], and is expected to be equal to $w_{ref} = 5.424{\times}10^{-3}$.

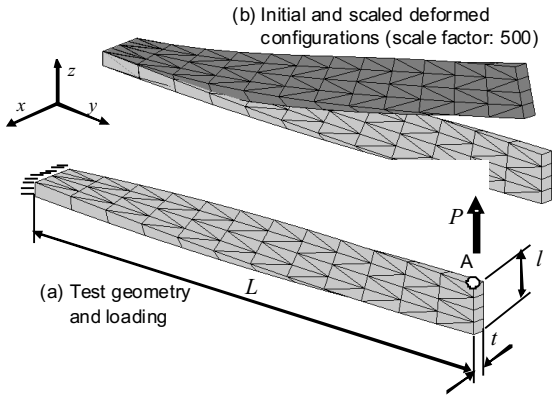


*Fig. 2.* Twisted beam: geometry, loading, boundary conditions, and example of a (12×4×1)×2 mesh

Table 2 shows the results for this test problem in terms of convergence as a function of the refinement of the mesh. The normalized displacements at point A in the loading direction $Oz$ are reported for three elements, using different mesh densities and only one

*Table 1.* Geometric, material, and loading data for the clamped circular plate problem

| | | |
|---|---|---|
| Length | $L$ | 12 |
| Width | $l$ | 1.1 |
| Thickness | $t$ | 0.32 |
| Young's modulus | $E$ | $29\times10^6$ |
| Poisson's ratio | $\nu$ | 0.22 |
| Applied load | $P$ | 1 |

element through the thickness. One can observe that element SHB6$^{bar}$ converges faster than elements SHB6 and PRI6.

*Table 2.* Normalized displacements in the z-direction at the load point A for the circular plate problem

| Mesh layout | PRI6 | SHB6 | SHB6$^{bar}$ |
|---|---|---|---|
| | $w/w_{ref}$ | $w/w_{ref}$ | $w/w_{ref}$ |
| (6×2×1)×2 | 0.061 | 0.234 | 0.496 |
| (12×4×1)×2 | 0.202 | 0.470 | 0.784 |
| (24×4×1)×2 | 0.485 | 0.779 | 0.935 |
| (36×8×1)×2 | 0.489 | 0.875 | 0.972 |

### 3.2. Circular plate subjected to a point load

This test problem of a clamped circular plate under a concentrated central load allows the performance of the element in bending and shearing to be assessed. Since the geometry, boundary conditions, and loading are symmetric, only one quarter of the plate is modeled using a $(3\times(N\times N\times1))\times2$ mesh nomenclature. Indeed, this quarter of the plate is divided into three zones containing $(N\times N\times1)\times2$ elements each (see Figure 3 for an example of a $(3\times(4\times4\times1))\times2$ mesh). The plate is subjected to a point load, $P = 1$, at the center, and is clamped on its edge. The geometric and material properties for this problem are described in Table 3. The reference central deflection in the $Oz$ direction is $w_{ref}$ = -2.65736×10$^{-5}$.

*Table 3.* Geometric, material, and loading data for the clamped circular plate problem

| | | |
|---|---|---|
| Radius | $R$ | 10 |
| Thickness | $t$ | 0.5 |
| Young's modulus | $E$ | $10^7$ |
| Poisson's ratio | $\nu$ | 0.25 |
| Applied load | $P$ | 1 |

The normalized deflections of the load point A in the $Oz$ direction are reported in Table 4 in terms of mesh refinement. As can be seen in this table, element SHB6$^{bar}$ converges towards the reference solution better than the two other elements SHB6 and PRI6.

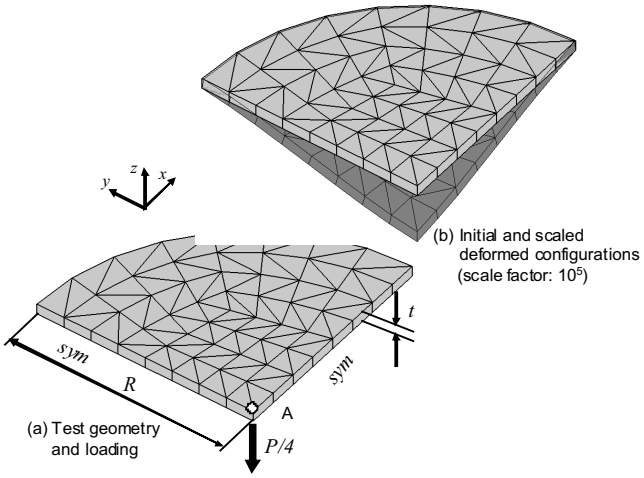


*Fig. 3.* Circular plate: Geometry, loading, boundary conditions, and example of a (3×(4×4×1))×2 mesh

*Table 4.* Normalized displacements in the z-direction at the load point A for the circular plate problem

| Mesh layout | PRI6 | SHB6 | SHB6$^{bar}$ |
|---|---|---|---|
| | $w/w_{ref}$ | $w/w_{ref}$ | $w/w_{ref}$ |
| (3×(2×2×1))×2 | 0.162 | 0.422 | 0.692 |
| (3×(4×4×1))×2 | 0.370 | 0.638 | 0.876 |
| (3×(6×6×1))×2 | 0.522 | 0.753 | 0.942 |
| (3×(8×8×1))×2 | 0.624 | 0.820 | 0.974 |

### 3.3. Pinched hemispherical shell with a mixture of elements

This test problem, which is often used to assess the three-dimensional inextensional bending behavior of shells, has become very popular and has been adopted by many authors since it was proposed by MacNeal and Harder [19]. This test is known to be severe because the transverse shear and membrane locking phenomena are dominant and are further accentuated by the particular geometry of the problem (distorted, skewed elements). This problem was studied in detail by Belytschko et al. [20], who showed that since all the elements are incurved in this doubly-curved shell problem, the intensity of membrane and shear locking is increased. Figure 4 shows the geometry, loading, and boundary conditions for this elastic thin shell problem (R/t = 250). In this example, a mixture of SHB6 and SHB8PS elements is used, in which the SHB6 elements are located at the top of the hemisphere.

Owing to the symmetry of the test, only one quarter of the hemisphere is meshed using a single layer of elements through the thickness and with two unit loads along the directions *Ox* and *Oy*. According to the reference solution [19], the displacement of point A along the *x*-direction is $w_{ref} = 0.0924$. Note that in order to compare the performance

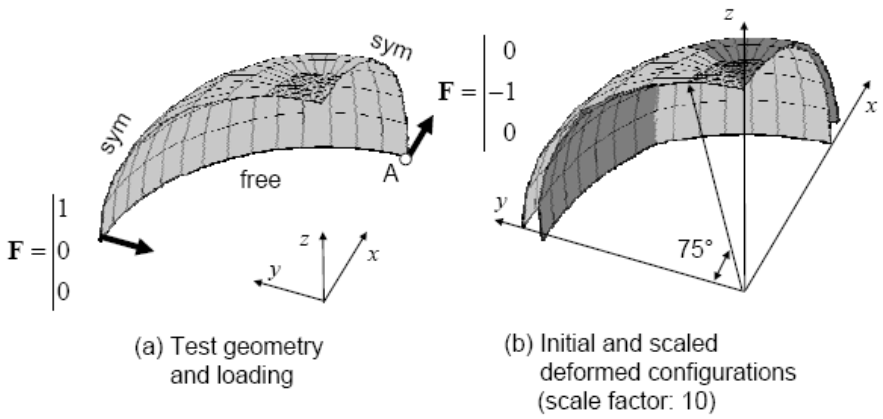


*Fig. 4.* Pinched hemispherical shell problem with a mixture of prismatic and hexahedral elements: the SHB6 elements are located at the top, and the SHB8PS elements are arranged over an angle of 75 °

*Table 5.* Geometric, material, and loading data for the pinched hemispherical shell problem

| | | |
|---|---|---|
| Radius | $R$ | 10 |
| Thickness | $t$ | 0.04 |
| Young's modulus | $E$ | $6.825\times10^7$ |
| Poisson's ratio | $\nu$ | 0.3 |
| Applied load | $F$ | 1 |

of solid–shell elements to that of standard three-dimensional elements, SHB6 elements are mixed with SHB8PS elements, and PRI6 elements are mixed with their three-dimensional counterpart HEX8, which are the standard, full integration eight-node hexahedral elements. The normalized results reported in Table 6 reveal a very good convergence rate when the SHB6 is mixed with the SHB8PS, which confirms the interest of mixing hexahedral and prismatic solid–shell elements.

*Table 6.* Normalized displacements at point A for the pinched hemispherical shell problem: mixed meshes.

| Number of elements | PRI6 + HEX8 | SHB6 + SHB8PS | $\text{SHB6}^{bar}$ + SHB8PS |
|---|---|---|---|
| | $w/w_{ref}$ | $w/w_{ref}$ | $w/w_{ref}$ |
| 36 | 0.001 | 0.703 | 0.785 |
| 100 | 0.002 | 0.880 | 0.960 |
| 156 | 0.004 | 0.929 | 0.983 |

## 4. CONCLUSIONS

A new solid–shell element SHB6$^{bar}$ has been developed and implemented into the finite element code ASTER. The key idea of this development is the adequate combination of a reduced integration rule with the well-known assumed-strain method. An interesting feature of this approach is the convenient fully three-dimensional framework on which this solid–shell element is based (six-node prism with only three translational degrees of freedom per node). Also it has been shown that no zero-energy modes arise from the adopted reduced integration scheme, and thus no stabilization procedure is required. As revealed by the benchmark problems, the SHB6$^{bar}$ element brings significant improvements compared to the standard three-dimensional six-node prismatic element denoted PRI6. The projection using the assumed-strain technique makes the quality of the element even better under combined bending and shearing. However, the convergence remains rather slow in some bending-dominated benchmark problems, probably due to constant strain states in linear triangular elements. This type of element blends naturally with the eight-node hexahedral solid–shell element SHB8PS, thus enabling one to analyze any structural geometry quite easily, which is the main motivation behind the development of the present SHB6$^{bar}$ element. Recall that meshing arbitrarily complex geometries is not permitted using only hexahedral elements.

## REFERENCES

[1] Belytschko T, Bindeman LP. Assumed strain stabilization of the eight node hexahedral element, *Computer Methods in Applied Mechanics and Engineering* **105** (1993) 225–260.

[2] Hauptmann R, Schweizerhof K. A systematic development of solid–shell element formulations for linear and non-linear analyses employing only displacement degrees of freedom, *International Journal for Numerical Methods and Engineering* **42** (1998) 49–69.

[3] Wall WA, Bischoff M, Ramm E. A deformation dependent stabilization technique, exemplified by EAS elements at large strains. *Computer Methods in Applied Mechanics and Engng.* **188** (2000) 859–871.

[4] Abed-Meraim F, Combescure A. SHB8PS a new adaptive, assumed-strain continuum mechanics shell element for impact analysis. *Computers & Structures* **80** (2002) 791–803.

[5] Legay A, Combescure A. Elastoplastic stability analysis of shells using the physically stabilized finite element SHB8PS, *International Journal for Numerical Methods and Engineering* **57** (2003) 1299–1322.

[6] Simo JC, Rifai MS. A class of mixed assumed strain methods and the method of incompatible modes, *International Journal for Numerical Methods and Engineering* **29** (1990) 1595–1638.

[7] Simo JC, Armero F. Geometrically non-linear enhanced strain mixed methods and the method of incompatible modes, *International Journal for Numerical Methods and Engineering* **33** (1992) 1413–1449.

[8] Simo JC, Armero F, Taylor RL. Improved versions of assumed enhanced strain tri- linear elements for 3D finite deformation problems, *Computer Methods in Applied Mechanics and Engng.* **110** (1993) 359–386.

[9] Dvorkin EN, Bathe KJ. Continuum mechanics based four-node shell element for general non-linear analysis, *Engineering Computations* **1** (1984) 77–88.

[10] Zhu YY, Cescotto S. Unified and mixed formulation of the 8-node hexahedral elements by assumed strain method, *Computer Methods in Applied Mechanics and Engng.* **129** (1996) 177–209.
[11] Wriggers P, Reese S. A note on enhanced strain methods for large deformations, *Computer Methods in Applied Mechanics and Engng.* **135** (1996) 201–209.
[12] Klinkel S, Wagner W. A geometrical non-linear brick element based on the EAS-method. *International Journal for Numerical Methods and Engineering* **40** (1997) 4529–4545.
[13] Klinkel S, Gruttmann F, Wagner W. A continuum based three-dimensional shell element for laminated structures. *Computers & Structures* **71** (1999) 43–62.
[14] Reese S, Wriggers P, Reddy BD. A new locking-free brick element technique for large deformation problems in elasticity, *Computers & Structures* **75** (2000) 291–304.
[15] Puso MA. A highly efficient enhanced assumed strain physically stabilized hexahedral element, *International Journal for Numerical Methods and Engineering***49** (2000) 1029–1064.
[16] Abed-Meraim F, Combescure A. An improved assumed strain solid–shell element formulation with physical stabilization for geometric nonlinear applications and elastic-plastic stability analysis, *International Journal for Numerical Methods in Engineering* 2009; doi:10.1002/nme.2676.
[17] Fish J, Belytschko T. Elements with embedded localization zones for large deformation problems, *Computers & Structures* **30** (1988) 247–256.
[18] Simo JC, Hughes TJR. On the variational foundations of assumed strain methods. *ASME Journal of Applied Mechanics* **53** (1986) 51–54.
[19] MacNeal RH, Harder RL. A proposed standard set of problems to test finite element accuracy, *Finite Elements in Analysis and Design* **1** (1985) 3–20.
[20] Belytschko T, Wong BL, Stolarski H. Assumed strain stabilization procedure for the 9-node Lagrange shell element, *International Journal for Numerical Methods in Engineering* **28** (1989) 385–414.

*Received October 14, 2009*

## PHẦN TỬ VỎ-KHỐI HÌNH LĂNG TRỤ MỚI "SHB6": CÔNG THỨC BIẾN DẠNG GIẢ ĐỊNH VÀ ĐÁNH GIÁ TRÊN CÁC BÀI TOÁN CHUẨN

Bài báo này đề nghị công thức cho phần tử vỏ-khối 6 nút, ký hiệu là SHB6. Phần tử lăng trụ này dựa trên phương pháp ba chiều thuần túy và vì thế chỉ có các chuyển dịch là các bậc tự do. Sử dụng lược đồ tích phân suy giảm với một điểm cầu phương trong mặt phẳng và một số tùy ý các điểm tích phân, tối thiểu là hai điểm, theo hướng "chiều dầy". Thêm vào đó, để làm tăng ứng xử của phần tử và giảm bớt đáng kể ảnh hưởng của nghẽn, các phép chiếu cụ thể được đưa vào trên cơ sở phương pháp biến dạng giả định. Kết quả thu được có thể sử dụng để mô hình các bài toán kết cấu mỏng có tính tới một số hiện tượng theo chiều dầy. Việc phân tích kỹ lưỡng hiện tượng có thể về suy giảm hạng ma trận độ cứng chỉ ra rằng không có mode "hourglass" nào cần kiểm soát. Tuy nhiên, nếu không sử dụng phương pháp biến dạng giả định phần tử có hiện tượng nghẽn trượt và loại nghẽn "dầy", các loại nghẽn thông thường của phần tử tuyến tính tam giác liên quan tới các trạng thái biến dạng phẳng. Sau khi trình bày chi tiết công thức, ứng xử của phần tử được đề cập qua một loạt các bài toán chuẩn nhằm minh họa cho khả năng của nó trong các tình huống khác nhau. Cụ thể hơn, phần tử vỏ-khối lăng trụ này chứng tỏ những ưu điểm cốt yếu so với phần tử lục giác SHB8PS trong việc tạo lưới cho các dạng hình học phức tạp tùy ý.